3906–3921 *Nucleic Acids Research, 2017, Vol. 45, No. 7* *Published online 4 February 2017*
doi: 10.1093/nar/gkx083

Tankyrase1-mediated poly(ADP-ribosyl)ation of TRF1 maintains cell survival after telomeric DNA damage

Lu Yang[1,2,3,†], Luxi Sun[1,2,3,†], Yaqun Teng[1,2,3], Hao Chen[1,2,3], Ying Gao[1,2,3], Arthur S. Levine[2,3], Satoshi Nakajima[2,3] and Li Lan[2,3,*]

[1]School of Medicine, Tsinghua University, No.1 Tsinghua Yuan, Haidian District, Beijing 100084, China, [2]University of Pittsburgh Cancer Institute; University of Pittsburgh School of Medicine; 5117 Centre Avenue, Pittsburgh, PA 15213, USA and [3]Department of Microbiology and Molecular Genetics; University of Pittsburgh School of Medicine; 450 Technology Drive, 523 Bridgeside Point II, Pittsburgh, PA 15219, USA

Received September 27, 2016; Revised January 09, 2017; Editorial Decision January 26, 2017; Accepted January 27, 2017

ABSTRACT

Oxidative DNA damage triggers telomere erosion and cellular senescence. However, how repair is initiated at telomeres is largely unknown. Here, we found unlike PARP1-mediated Poly-ADP-Ribosylation (PARylation) at genomic damage sites, PARylation at telomeres is mainly dependent on tankyrase1 (TNKS1). TNKS1 is recruited to damaged telomeres via its interaction with TRF1, which subsequently facilitates the PARylation of TRF1 after damage. TNKS inhibition abolishes the recruitment of the repair proteins XRCC1 and polymerase β at damaged telomeres, while the PARP1/2 inhibitor only has such an effect at non-telomeric damage sites. The ANK domain of TNKS1 is essential for the telomeric damage response and TRF1 interaction. Mutation of the tankyrase-binding motif (TBM) on TRF1 (13R/18G to AA) disrupts its interaction with TNKS1 concomitant recruitment of TNKS1 and repair proteins after damage. Either TNKS1 inhibition or TBM mutated TRF1 expression markedly sensitizes cells to telomere oxidative damage as well as XRCC1 inhibition. Together, our data reveal a novel role of TNKS1 in facilitating SSBR at damaged telomeres through PARylation of TRF1, thereby protecting genome stability and cell viability.

INTRODUCTION

One of the most important cellular challenges is the maintenance of genome stability. Single strand breaks (SSBs) are the most frequent type of DNA damage, occurring at a frequency of tens of thousands per cell per day (1). Defects in efficient SSB repair (SSBR) are implicated in a variety of diseases such as neurodegenerative disorders, premature aging and cancer (1). Therefore, cells have evolved rapid and efficient repair mechanism for SSBs (1). Poly(ADP-ribose) polymerase 1 (PARP1) is a DNA nick sensor protein which binds to DNA strand breaks efficiently and adds poly-ADP-ribose (PAR) to various target proteins using NAD^+ as a substrate to facilitate DNA repair (2–4). PARylation amplifies damage signals within chromatin, recruiting repair proteins, including XRCC1, to the damage sites; XRCC1 is a molecular scaffold involved in SSBR. Although PAR has a rapid turnover mediated by PARG after its formation, XRCC1 is retained at the damage sites together with its interacting repair components such as polymerase β (Polβ) to complete the repair process (3,5–7). PARP inhibitors sensitize cells to radio- and chemotherapeutic agents, showing the importance of PAR in maintaining cell viability (2,3,8,9).

Preventing chromosome ends from being recognized as double-strand breaks (DSBs) by the DNA repair machinery is important for maintaining genome stability and cell survival. Mammalian cells have evolved unique nucleoprotein complexes at telomeres to solve this 'end protection' problem (10,11). Human telomeres typically consist of a repeating array of duplex TTAGGG sequences ending with a 3′ 130–210 nucleotide protrusion of single-stranded TTAGGG repeats (12). The 3′ overhang can fold back and invade into the double stranded telomeric repeats by base pairing with the C-rich strand to form a T-loop structure (13). Telomeres are capped by a six-subunit protein complex called the shelterin complex (14,15). Of the six subunits, TRF1 and TRF2 have a relatively high abundance and form a homodimer which bind to telomeric duplex DNA in a sequence-specific manner (16–18). Dysfunctional telomeres caused by critically shortened telomeres or lack of protection by the shelterin complex activate the canonical DNA damage response (DDR) pathway that engages p53 to initiate apoptosis or replicative senescence (10,19–22).

*To whom correspondence should be addressed. Tel: +1 412 623 3228; Fax: +1 412 623 7761; Email: lil64@pitt.edu
†Authors contributed equally.

Telomeres are shortened with each cell division due to the requirement of a labile primer for DNA polymerase to initiate unidirectional 5′→3′ synthesis, which leaves the 3′ end of the template not fully replicated (23). The process of telomere shortening and erosion is accelerated by oxidative stress (24). Although exposed to increased replicative stress and oxidative stress, cancer cells maintain immortality by achieving telomere elongation via two distinct pathways, one that is telomerase-dependent or one that is telomerase-independent; the latter is also referred to as alternative lengthening of telomeres (ALT). During oxidative stress, the accumulation of 8-oxoG and SSBs is more likely to occur at telomeres than at the bulk of the genome due to the high ratio of guanine residues in telomeric repeat sequences (25). Moreover, previous reports have shown that oxidative DNA damage is repaired less efficiently at telomeres than the rest of the genome *in vitro* (26), suggesting that repair at telomeres may be affected by its unique structure. Due to lack of an effective system to induce telomere-specific DNA damage *in vivo*, it has remained unclear as to how SSBR is initiated and processed at damaged telomeres given the protection of the shelterin complex and the high-order telomere structure in telomerase-positive and ALT cells.

To address this question, we used a KillerRed (KR)-based system to induce localized oxidative DNA damage at telomeric or non-telomeric regions (24,27). Previous investigation of telomere damage and repair using shelterin knock-outs or by introducing DNA nuclease at telomeres may not have accurately represented the common situation that cells encounter, in that oxidative damage is the major form of DNA damage from the environment. KR is a unique fluorescent protein which generates superoxide upon light illumination at a given range of wavelength (550-580 nm) (28–30), mimicking natural oxidative damage and its consequent DNA strand breaks. In this study, we discovered a novel function of tankyrase1 (TNKS1) which initiates telomere SSBR. Tankyrase1 belongs to the poly (ADP-ribose) polymerase (PARP) superfamily, which consists of 18 proteins with a C-terminal conserved catalytic domain similar to its founding member, PARP1 (31). Unlike the role of Tankyrase1 (TNKS1, PARP5a) in regulating telomere length by allowing the access of telomerase (32,33), we found that recruitment to telomere damage sites of TNKS1 is dependent on its interaction with TRF1; this is independent of either telomerase or the cell cycle. Importantly, we have defined the key residues on TRF1 at its N-terminal RGCADG motif which are critical for the interaction with TNKS1. Impairment of the recruitment or function of TNKS1 at telomeres greatly increases genome instability and sensitizes cells to telomere oxidative damage. Here we present evidence that TNKS1 and PARP1 provide differential functions in PARylation at distinct damage sites. Together, our results demonstrate a location-defined mechanism for SSBR initiation at telomeric vs. non-telomeric regions upon oxidative damage.

MATERIALS AND METHODS

Cell lines and transfections

U2OS, HeLa, HeLa1.3 and Flip-in T-REX 293 cells were propagated in Dulbecco's modified Eagle's medium (DMEM; Lonza) supplemented with 10% FBS at 37°C, 5% CO_2. Flip-in 293 shTRF1 cells were maintained in DMEM supplemented with 10% FBS and 1 μg/ml Puromycin. KR-TRF1, RFP-TRF1 or NLS-KR stably expressing Flip-in T-REx 293 cell lines (tet-on) were established by transfection of pcDNA5/FRT/TO RFP-TRF1, KR-TRF1 and NLS-KR, respectively, with 150 μg/ml Hygromycin B (Sigma) selection. Induction of expression in Flip-in T-REX 293 cells was done by adding 2 μg/ml tetracycline (Sigma) 24 hr before induction. Plasmids were transfected with lipofectamine 2000 (ThermoFisher Scientific) according to the manufacturer.

Plasmids

KR and RFP with additional Age I and EcoRI sites were amplified by PCR and sub-cloned into a pYFP (Clontech) tagged TRF1 plasmid to generate pCMV KR-TRF1 and RFP-TRF1 plasmids. KR-TRF1 and RFP-TRF1 fragments were digested from pCMV-KR-TRF1, pCMV-RFP-TRF1 and pCMV-DsR-TRF1 constructs by KpnI and SmaI and sub-cloned into the KpnI- EcoRV sites of pcDNA5/FRT/TO (Invitrogen), respectively. pcDNA5/FRT/TO NLS-KR was made by PCR of KR with an additional nuclear localization signal in front of the KpnI site and an EcoRV site using 5′-ATGGTACCATGGATCCAAAAAAGAAG-3′and 5′-GCGATATCCTAGATTTCGTC G-3′ as forward and reverse primers, respectively, and sub-cloned into the KpnI and EcoRV sites of the pcDNA5/FRT/TO vector. Truncations of TNKS1 were obtained by PCR using FLAG-TNKS1 as a template. Amplified fragments with an additional XhoI site at 5′ and NotI at 3′ ends were cloned into a pEGFP-C1 vector (Clontech). The TRF1 TBM1 mutant fragment was first amplified by PCR using 5′ primer containing mutation sites and a 3′ primer with a NotI site. Then the PCR product served as a template to amplify the full length TBM1 mutant using a TRF1 5′ primer with a SalI site and a TRF1 3′ primer with a NotI site. The mutant was cloned into a pBS vector and selected with a Blue/white selection system. pEGFP-XRCC1, its deletion mutants, and GFP-53BP1 and Pol β were described previously (5). The pBS-TRF1 TBM1 mutant construct was then subcloned into the SalI-NotI sites of a pcDNA/FRT/TO/Flag-His vector (Invitrogen). Primers used in PCR are listed below: ANK forward primer: 5′-CCGCTCGAGATGGCGGCGTCGCGTC-3′; ANK reverse primer: 5′-TATTTGCGGCCGCA CATTGGAGGCTCCT-3′; SARP forward primer: 5′-CCGCTCGAGGCCTCTCTGATCTCACCAGC-3′; SARP reverse primer: 5′-ATAAGAATGCGGCCGCAG GTCTTCTGCTCTGCGG-3′; PARP forward primer: 5′-CCGCTCGAGGGTGGACAACAAGGCACCAA-3′; PARP reverse primer: 5′ ATAAGAATGCGGCCGCAG GTCTTCTGCTCTGCGG-3′; TBM1 fragment forward primer: 5′-GCGGCCCCGAGCCCGGCCGGCTGT

GCGGATGCTAGGGAT-3′; TBM1 fragment reverse primer: 5′-TTTGCGGCCGCAGTCTTCGCTGTCTG AGGAAATCAG-3′; TBM1 full length forward primer: 5′-TTTTCTCGAGATGGCGGAGGATGTTTCCTCA-3′; TBM1 full length reverse primer: 5′-TTTGCGGCCGCA GTCTTCGCTGTCTGAGGAAATCAG-3′

Chemicals and RNA interference

The PARP inhibitors PJ34 (Sigma) and Olaparib (Selleckchem) with a final concentration of 4 and 10 μM were added into medium for 30 min, respectively. The tankyrase 1/2 inhibitor VI G007-LK (Millipore) was used with a 92 nM final concentration in medium for 24 h; XAV939 (Tocris) was added with a final concentration of 20 M for 24 h. Induction of Flip-in T-REX 293 KR-TRF1 expression was done by adding 2 g/ml tetracycline (Sigma). The PARG inhibitor ADP-HPD, dihydrate ammonium salt (CALBIOCHEM), was added to lysis buffer with a 1 μM final concentration. The siTNKS1, 5'-AACAAUUCACCGUCGUCCUCUU-3', was used in this study. siTNKS1 was transfected into U2OS cells at a final concentration of 25 pmol/ml 48 h before analyzing the cells. Two TRF1 siRNA sequences targeting 3′UTR were used in imaging and the survival study of the TRF1 TBM1 mutant: 1.AGAGUAACCUAUAAGCAUG (J-010542-07-0005, Dharmacon), 2.UACCAGAGUUAAAGCAUAU (J-010542-08-0005, Dharmacon). The two sequences were mixed in a 1:1 ratio and transfected to cells 48 h before analyzing. For imaging, siRNAs were co-transfected with plasmids at a final concentration of 40 pmol/ml using lipofectamine 2000, 24 or 48 h prior to light exposure. For the survival assay, siRNAs were transfected at a final concentration of 50 pmol/ml using the DharmaFECT transfection reagent (GE Dharmacon) 48 h prior to cell seeding at a final concentration of 50 pmol/ml.

KR activation

KR activation was conducted in two ways. Activation of KR in a single cell was performed with a 559 nm laser for 20 scans (1 mW/scan) only for the selected cell nucleus. Local activation of one KR spot was performed with the same 559 nm laser in a selected area within a single cell nucleus. One scan takes less than 1 second. Activation of KR in bulk cells was done by exposing cells to a 15 W SYLVANIA cool white fluorescent bulb for the indicated time (20 min to 4 h) in a stage UVP (Uvland, CA, USA). The dose of 559 nm laser light that was delivered to the KR spot has been calculated. The KR-TRF1 (∼1 μm^2 in diameter) spot is ∼12 $mJ/\mu m^2$. In the case of fluorescent light activation, the rate of light is 15 $J/m^2/s$. With a 20 min–1 h light exposure, the final power delivered to each KR-TRF1 spot is around 20–60 $mJ/\mu m^2$ upon light exposure. Cells were placed under a water bottle (height to light is 15 cm) to prevent an increase of temperature during light activation.

Immunoprecipitation and western blot analysis

Lysates were prepared using 250 mM low salt lysis buffer (250 mM NaCl, 10 mM HEPES, 50 mM Tris–HCl 7.4, 0.1% NP40, 5 mM EDTA) supplemented with protease inhibitor cocktail (Sigma) and PMSF (final 1 mM). Lysate was incubated overnight at 4 degrees with Flag M2 beads (Sigma) under continuous rotation. After four times washing in lysis buffer, proteins were eluted in 3* loading buffer and subjected to SDS-PAGE and western blotting. Western blotting was performed using standard methods. Blots were incubated with primary antibodies using anti-Flag M2 antibody (scientific imaging system, IB13026/8J2731), GFP (Roche Diagnostics), TNKS (Santa Cruz), and tubulin. After incubation with horseradish peroxidase-linked secondary antibodies (Jackson Immunosciences), the blots were developed using the chemiluminescence detection kit ECL-Plus according to the manufacturer's instructions. Quantification was performed on scanned images of blots using the Image Lab software, and the values shown on the graphs represent normalization of the protein content evaluated through tubulin immunoblotting.

Confocal microscopy

The Olympus FV1000 confocal microscopy system (Cat. F10PRDMYR-1, Olympus) with a FV1000 SIM Scanner and 405 nm laser diode (Cat. F10OSIM405, Olympus) was employed. FV1000 software was used for acquisition of images. For inducing DNA damage, a 405 nm laser was used with the indicated power; the output power of the 405 laser passed through the lens is 5 mW/scan. Laser light was passed through a PLAPON 60× oil immersion objective lens (super chromatic abe. corr. obj W/1.4NA FV, Cat. FM1-U2B990). Cells were incubated at 37°C on a thermoplate (MATS-U52RA26 for IX81/71/51/70/50; metal insert, HQ control, Cat. OTH-I0126) in Opti-MEM during observation to avoid pH changes. For bleaching KR, a 559 nm laser was used. For counting foci positive cells, cells containing >5 colocalized foci with KR-TRF1 were counted. For calculation of the percentage of colocalization with KR-TRF1, foci positive cells in 50 cells were counted in every experiment. Three independent experiments were performed, and representative data are shown. Fluoview Soft (Olympus) was used for data analysis. In cases of quantification of the intensity of the damage response of proteins, a ratio of enrichment of the same area in a single cell nucleus was used. Here, mean intensity of accumulated proteins at the sites of KR-TRF1/mean intensity of proteins distant from the KR-TRF1 spot (background) in the same nucleus was calculated. Fifty spots in 10 cells were calculated. The ±SD calculated in each case is shown in the Figure Legend. The *P* value is calculated by student's t-test using Stat Plus software; $P<0.005$ is shown as **.

Method for the statistical analysis of the recruitment

Colocalization analysis in Olympus Fluoview software was used to analyze the recruitment of proteins of interest to the damaged telomeres. In each group, telomeres in over 10 cells were calculated. Pixels in each selected telomere were plotted onto a scattered graph based on the intensity of the two channels. Each telomere gives a Pearson co-efficiency number based on the plot. The Pearson co-efficiency is cal-

culated by

$$r = r_{xy} = \frac{\sum x_i y_i - n\bar{x}\bar{y}}{\sqrt{\left(\sum x_i^2 - n\bar{x}^2\right)}\sqrt{\left(\sum y_i^2 - n\bar{y}^2\right)}}$$

Clonogenic assay

U2OS or HeLa cells were seeded into a 35 mm dish. siRNA was transfected into cells using DharmaFECT transfection reagent (GE Dharmacon, T-2001-03) according to the manufacturer. Twenty-four hours post-siRNA transfection, plasmids were transfected into cells using lipofectamine 2000 reagent (Invitrogen, 11668019) according to the manufacturer. Seven hours post-plasmid transfection, cells were seeded into a 60 mm dish at a density of 300 cells/dish in dim light. Twelve-sixteen hours post-seeding, cells were exposed to light to induce KR-TRF2-induced telomere-specific damage. After 10 days of incubation in the dark, cells were washed once with PBS and then fixed and stained with 0.3% crystal violet in methanol. Colony numbers were counted and standardized vs. an untreated control group to test cell viability.

MTT assay

Flip-in T-REX 293 cells that stably expressed KR-TRF1, RFP-TRF1 or NLS-KR, respectively, with tetracycline induction, were seeded in 60 mm dishes. Cells were transfected with or without siTNKS1 24 h post-seeding. One day after siTNKS1 transfection, tetracycline was added with a concentration of 2 μg/ml in media for another 24 h followed by treatment for the indicated time period of light exposure. Cells were reseeded at a density of 5×10^3 cells per well of 96-well plates immediately after light treatment. Cell viability was determined 48 h after light activation with an MTT assay Kit (Promega). Absorbance was measured at 490 nm on a 96-well plate reader (VERSAmax tunable microplate reader, Molecular Devices). Results are presented as a percentage of survival taking the control (untreated cells) as 100% survival.

Metaphase chromosome spreads and telomere FISH

KR-TRF1 or DsR-TRF1 stably expressing HeLa1.3 cell lines were treated with DMSO, or Olaparib (Selleckchem) with a final concentration of 10 μM for 30 min, or XAV939 at a final concentration of 5 uM for 6 h. Cells were then exposed to 15 W white light for 1 h. After incubation for 12 h in the dark, cells were arrested at metaphase with 0.1 ug/ml colcemid (Sigma) for 5 h. Cells were harvested by gentle pipetting and swollen in 0.075 M KCl at 37°C for 30 min. Cells were then fixed in fixative (3:1 methanol/glacial acidic acid) for three times, each for 10 min. Cells were dropped onto wet slides and air-dried overnight in preparation for telomere-PNA FISH analysis. The next day, the slides were rehydrated with PBS for 5 min and fixed with 3.7% formaldehyde for 10 min at room temperature. After three PBS washes, the slides were treated with RNase A (0.1 mg/ml) in PBS at 37°C for 10 min. Slides were then incubated consecutively with 75%, 85%, and 100% ethanol and allowed to air dry for at least 30 min before applying hybridization solutions (70% formamide, 0.1% BSA, 0.5ug/ml yeast tRNA, 0.1*SSC) containing TelC-Cy3-PNA probe (PANAGENE, F1002). Slides were denatured by heating for 3 min at 80°C and hybridized for 2 h at 37°C. Following hybridization, the slides were washed twice for 15 min each in 70% formamide/10 mM Tris-HCl, followed by three 5 min washes in 0.1 M Tris–HCl, pH 7.0/0.15 M NaCl/0.08% Tween-20. The chromosomal DNA was counterstained with 4,6-diamidino-2-phenylindole (DAPI) applied to the second wash. Slides were air dried and mounted in mounting medium and sealed with nail oil.

Cell cycle synchronization and imaging

Normal DMEM + 2.5 mM thymidine was added to a 50% confluency of U2OS cells for 24 h; then thymidine was removed by washing with 1× PBS, fresh DMEM was added, and the cells were transfected with RT1/KT1 with lipofectamine 2000. Eight hours post-transfection, HU (2 uM) was added to cells. After 16 h incubation, cells were released by removing the drug, washing with 1× PBS and adding fresh medium. Cells were fixed by 4% PFA after 0, 4 and 8 h to obtain G0/G1, S and G2/M phase cells, respectively. For immunostaining and imaging, cells were exposed to light for 20 min and recovered for 30 min in the dark before fixation to induce oxidative telomeric damage. After fixation, cells were permeabilized by 0.2% Triton X-100, blocked with 2% BSA and incubated with γH2AX Ab, TNKS Ab for immunofluorescence and confocal imaging.

RESULTS

Kinetics of PARylation at the non-telomeric and telomeric region after damage

To identify if SSBR is initiated and processed by the same mechanism at telomeres which form heterochromatin structure, versus non-telomeric heterochromatin regions, we utilized a KR-based assay to induce location-defined oxidative damage at these sites. KR was either fused to the tet repressor (tetR-KR) to target a defined non-telomeric heterochromatin locus that contains chromosomally integrated tetracycline response element (TRE) repeats (27) or fused to TRF1 or TRF2 (KT1 or KT2) to target telomeres (Figure 1A). The table in Figure 1A briefly shows the methods we used to induce site-specific oxidative damage and the KR controls DsRed-TRF1/TRF2 (DT1 or DT2) and RFP-TRF1/TRF2 (RT1 or RT2). Both KT and the non-damage controls display telomere-specific localization, as shown by their colocalization with telomeric peptide nucleic acid (PNA) probes (Supplementary Figure S1A). KR activation was induced by a 15 W Sylvania cool white fluorescent bulb for 20 min as described in a previous study (24). KR-induced oxidative DNA damage is site-specific, since the chromophore binds to the surrounding hydrophobic residues, preventing the released superoxide from dispersing throughout the nucleus (34). The production of oxidative damage at telomeres was confirmed using the spin trap, 5,5-dimethyl-pyrroline N-oxide (DMPO), which binds and reacts with multiple free radicals (e.g. superoxide and hydroxyl radicals) to form stable and distinguishable free

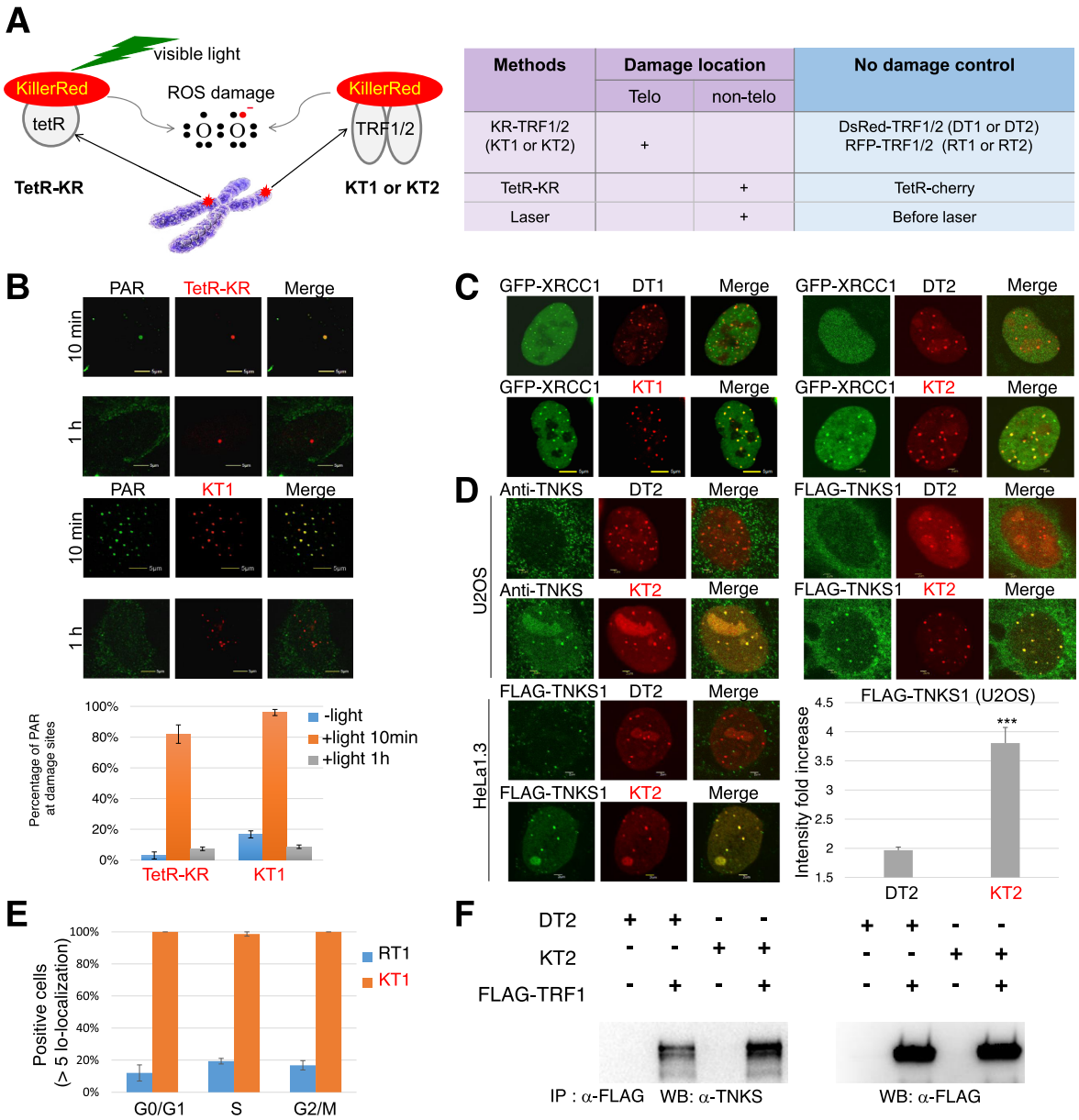

Methods	Damage location		No damage control
	Telo	non-telo	
KR-TRF1/2 (KT1 or KT2)	+		DsRed-TRF1/2 (DT1 or DT2) RFP-TRF1/2 (RT1 or RT2)
TetR-KR		+	TetR-cherry
Laser		+	Before laser

Figure 1. TNKS1 is recruited efficiently at telomeric oxidative damage sites. (**A**) Scheme of the methods: DNA damage Targeted at one Genome locus by tetR-tagged KillerRed (tetR-KR) and at telomeres by KillerRed tagged TRF1 or TRF2 (KT1 or KT2), respectively. KillerRed (KR) induces localized reactive oxygen species (ROS) damage after visible light activation either at one genome locus or telomeres. DsRed-TRF1/2, RFP-TRF1/2 is used for a no damage control at telomeres. TetR-cherry is the no damage control for Tet-KR at one genome locus. 405 nm laser micro-irradiation is also used for inducing genomic damage. (**B**) Kinetics of PAR at sites of tetR-KR or KT1 transfected U2OS (TRE) cells with or without light activation. Cells were exposed to light for 20 min and recovered in the dark for the indicated time. Quantification of the percentage of cells showing co-localization of PAR with tetR-KR or KT1 spots, respectively, is shown. (**C**) GFP-XRCC1 is recruited efficiently to either KT1 or KT2 induced telomeric oxidative damage sites but not to DT1 or DT2 undamaged controls. (**D**) Recruitment of endogenous tankyrase and FLAG-TNKS1 greatly increased upon telomere damage. U2OS cells were stained with α-TNKS Ab after 15 W SYLVANIA cool white fluorescent light exposure for 20 min and recovery in the dark for 30 min. U2OS or HeLa 1.3 cells were co-transfected with FLAG-TNKS1 and DT2/KT2 and stained with FLAG Ab after light exposure for 20 min and recovery in the dark for 30 min. Intensity fold increase defined by the foci intensity normalized to background is quantified in U2OS cells transfected with FLAG-TNKS1. The error bar represents over 300 foci. (**E**) U2OS cells transfected with RT1/KT1 and synchronized by a double thymidine block to different cell stages were exposed to light for 20 min and recovered in the dark for 30 min before fixation. Cells were stained with TNKS Ab and imaged with a confocal microscope. Cells showing >5 foci of co-localization were defined as positive cells. The error bar represents three independent experiments with 50 cells in each. (**F**) The interaction between TRF1 and TNKS1 is greatly enhanced with induction of telomere oxidative damage. 293 cells were co-transfected with FLAG-TRF1 or vector together with DT2 or KT2. Cells were exposed to light for 1 hr before being harvested for co-immunoprecipitation. FLAG M2 beads were used for IP and the precipitates were subjected to electrophoresis and immunoblotted with α-TNKS and α-FLAG Ab.

radicals (35). We observed co-localization of DMPO with KT1 spots upon light activation, suggesting that the KT1 released superoxide is restricted to the telomeres (Supplementary Figure S1B). The frequency of cells showing co-localization of PAR and 8-oxo-Guanine (8-oxoG), a major lesion caused by oxidative DNA damage, dramatically increased from <20% to over 90% at KT1 spots upon light activation, while this colocalization was seldom detected in DT1/RT1 expressing cells with or without light exposure (Supplementary Figure S1C and D). This result reinforces the conclusion that oxidative DNA damage is specifically and efficiently induced at sites of telomeres after KR activation.

Given the importance of PARylation to initiate SSBR at DNA damage sites, we investigated the kinetics of PARylation at telomeres after damage induction. As shown in Figure 1B, at both non-telomeric (tetR-KR) and telomeric (KT1) damage sites, PAR is generated extensively 10 min after damage induction, and is degraded within 1 h. In addition, we found that XRCC1 is similarly recruited to both KT1 and KT2 induced telomeric damage following PAR formation (Figure 1C), indicating that telomeres and non-telomere DNA may employ a similar repair mechanism for SSBs and PAR might be important for SSBR at telomeres.

TNKS1 is preferentially recruited to telomeres after damage

Next we investigated how PAR is synthesized at damaged telomeres. In spite of the fact that PARP1 is considered the major enzyme responsible for over 90% PARylation *in vivo*, TNKS1 has been found to interact with TRF1 (32,33,36), suggesting that TANKS1 might have a specific role in telomere damage repair. We tested the recruitment of TNKS1 at KT1 induced telomere damage sites and found that FLAG-TNKS1 could be recruited to KT1 damaged sites and partially recruited to RT1 undamaged sites in U2OS cells (Supplementary Figure S2A). To exclude the effect of TNKS1 and TRF1 overexpression, we tested the recruitment of endogenous tankyrase to KT1 damage sites or used KT2 instead to induce telomere oxidative damage. KT2-mediated telomere oxidative damage is confirmed by its localization at telomeres and its ability to recruit XRCC1 as efficiently as KT1 (Figure 1C). We found that both endogenous tankyrase and FLAG-TNKS1 co-localized with KT2 damage sites but not the DT2 undamaged control in both U2OS (ALT) and HeLa1.3 cells (telomerase positive) (Figure 1D). The foci intensity of FLAG-TNKS1 at KT2 sites in U2OS cells was almost twofold stronger compared to the DT2 undamaged control (Figure 1D). Also, endogenous tankyrase was recruited efficiently to KT1 damage sites but not RT1 (Supplementary Figure S2B). Considering the cell cycle-dependent localization of TNKS1 in cells (37), we then synchronized cells to different cell cycle stages and tested the recruitment of endogenous tankyrase to telomeric oxidative damage induce by KT1. As shown in Figure 1E, although the basal level of tankyrase at telomeres without damage (RT1) showed a little increase (from about 10% to 20%) at S and G2/M phases compared to the G0/G1 phase, the frequency of tankyrase co-localized with KT1 dramatically increased to nearly 100% in all cell stages. Consistent with the damage recruitment of TNKS1, the interaction between TNKS and TRF1 showed a clear increase with the induction of telomere oxidative damage (Figure 1F). In contrast to KR-induced oxidative damage at telomeres, disrupting the shelterin complex by treating cells with either siTRF1 or siTRF2 did not trigger the recruitment of TNKS1 to telomeres (Supplementary Figure S2C), indicating that the recruitment of TNKS1 is specific to oxidative damage but not to shelterin depletion-mediated telomeric structural disruption. Together, our results suggest a role of TNKS1 in telomere oxidative damage repair which is independent of telomerase and the cell cycle.

PARP1 plays a central role in producing PAR at sites of DNA damage induced by laser irradiation or tetR-KR after light illumination (27). In contrast, the recruitment of PARP1 to telomeric damage sites only shows a slight increase compared to DT2 undamaged sites, which is statistically non-significant (Supplementary Figure S2D). On the other hand, the recruitment of TNKS1 to non-telomeric damage induced by laser microirradiation or tetR-KR is hardly detected (Supplementary Figure S2E). A previous study showed that when a nuclear localization signal (NLS) was fused to TNKS, overexpressed TNKS1 was recruited to I-sce1-induced DSBs and 800 nm multiphoton laser striping (38). The NLS might change the physiologic context in the cell, since TNKS1 is mainly located in the cytoplasm in G1 phase cells in our and a previous study (37). Our results indicate that TNKS1 was not recruited efficiently to non-telomeric oxidative damage sites and its consequent SSBs, while a role of TNKS1 in the repair of DSBs is not excluded. A summary of the recruitment of PARP1 and TNKS1 to KT1, tetR-KR and 405 nm laser-induced DNA damage (Supplementary Figure S2F) indicates the preferential recruitment of TNKS1 to telomeric and PARP1 to non-telomeric oxidative damage, respectively.

TNKS1 is responsible for PARylation of TRF1 after damage

The affinity of TNKS1 for telomeres indicated that it might be the major enzyme contributing to PARylation at telomeric SSBs. Thus, we tested if the PAR generated at telomere damage sites is mediated by TNKS1 with several PARP inhibitors. Olaparib specifically suppresses the catalytic activity of PARP1/2. G007-LK and XAV939 are tankyrase specific inhibitors (39,40). PJ34 is a general PARP inhibitor which has low selectivity. As shown in Figure 2A, we found that inhibition of tankyrase significantly abolished generation of PAR at telomere damage sites (Figure 2B). However, PARylation at non-telomeric damage sites induced by tetR-KR was not affected by tankyrase inhibitors (Supplementary Figure S3A), suggesting a difference in the mechanism of damage-induced PARylation at telomeric and non-telomeric damage sites.

We then tested if TRF1 is PARylated by TNKS1 when damage is induced in stable tetracycline-inducible KT1 293 cells. The scheme of the experiment is shown in Figure 2C, upper panel, and the inducible expression pattern of KT1 is confirmed by a western blot (Supplementary Figure S3B). Immunoprecipitation of TRF1 indicated that the TRF1 complex was PARylated when telomere oxidative damage was induced (Figure 2C, lanes 1 and 2). However, this PARylation of TRF1 was greatly reduced when cells

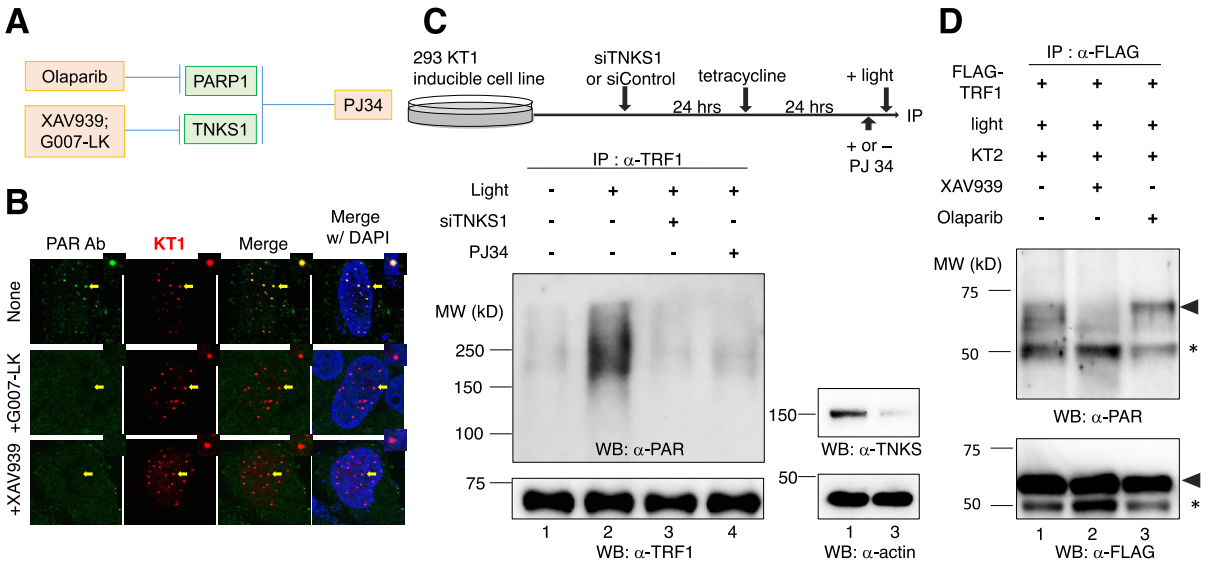

Figure 2. PARylation of TRF1 at telomere damage sites is mediated by TNKS1. (**A**) Schematic illustration of PARP inhibitors. (**B**) PAR at KT1 damage sites is blocked by G007-LK and XAV939. Cell were treated with a tankyrase inhibitor, 92 nM G007-LK, for 24 h and 20 μM XAV939 for 24 h, followed by 30 min of 559 nm laser light to activate KR to induce telomeric damage. (**C**) Schematic representation of experimental procedure for IP. PARylation of TRF1 is induced by telomeric oxidative damage and inhibited by tankyrase inhibitors. KT1 stably expressing Flip-in T-REX 293 cells were treated with or without siTNKS1 or 4 μM PJ34 for 30 min. Cell lysates were collected with a lysis buffer containing 960 μM of the PARG inhibitor, ADP-HPD, dihydrate ammonium salt, immediately after light exposure for 10 min and immunoprecipitated with α-TRF1. The precipitates were immunoblotted with α-pAR and α-TRF1. (**D**) PARylation of TRF1 after telomere damage is blocked by a TNKS inhibitor but not a PARP1 inhibitor. 293 cells were transfected with FLAG-TRF1 together with KT2. Cells were exposed to light for 20 min before harvest. Cell lysates were collected with a lysis buffer containing 960 μM of the PARG inhibitor and immunoprecipitated with α-FLAG. The precipitates were subjected to electrophoresis and immunoblotted with α-pAR and α-FLAG.

were treated with either siTNKS1 or PJ34 (Figure 2C, lanes 3 and 4).

To further confirm the result, we expressed KT2 in 293 cells to induce telomere oxidative damage. We found that the tankyrase specific inhibitor XAV939 greatly reduced the PARylation level on TRF1 (Figure 2D, lanes(1 and 2). However, treatment with the PARP1 inhibitor Olaparib does not have any effect on TRF1 PARylation upon telomere oxidative damage (Figure 2D, lane 1 and 3). This is consistent with a previous *in vitro* PARP assay showing that TRF1 did not serve as an acceptor of ADP-ribosylation by PARP1 (33). These results together indicated that TRF1 is PARylated upon telomere damage and this PARylation is mediated by TNKS1.

TNKS1 is required for maintaining genome stability and cell viability after induction of telomere oxidative damage

To reveal the biological effect of TNKS1 in the telomere damage response, we treated cells with siTNKS1 and tested cell viability in response to telomere oxidative damage induced by KT1/KT2 in both ALT cells and telomerase-positive cells. We found that TNKS1 deprivation sensitized cells to telomere oxidative damage in both ALT cells (Figure 3A) and telomerase-positive 293 and HeLa cells (Figure 3B and C). A low dose sensitization was observed in 293 and ALT cells upon damage, probably due to very efficient low dose light induced SSBs, without much production of DSBs (Figure 3A, B). In contrast, PARP1 suppression leads to increased sensitivity under low dose light (Figure 3A). It is notable that ALT cells showed greater sensitivity to telomere oxidative damage compared to telomerase-positive cells, suggesting that the increased cell death in TNKS1 knockdown (KD) cells is independent of its role in regulating telomere length through the telomerase-dependent pathway. To further this observation, we treated HeLa cells with siTNKS1 together with the telomerase inhibitor BIBR1532. The combined treatment sensitized HeLa cells to telomere oxidative damage to a similar extent as with U2OS cells (Figure 3C), suggesting that telomerase may not simply be a reverse transcriptase functioning in telomere elongation; it may also have a protective role in the telomere damage response.

To understand the effects of TNKS inhibition on genome stability, we performed metaphase spreads and a PNA FISH assay after induction of telomere damage by KT1 followed by recovery in the dark for 12 h, with or without TNKS inhibition. Examples of telomere aberrations and chromosome aberrations found in each group are shown in Figure 3D. Genome stability was scored by quantifying the frequency of these aberrations. As shown in Figure 3E, treatment with a TNKS inhibitor or induction of telomere oxidative damage caused increased aberrations compared with a control group. The frequency of each type of aberration is shown in Supplementary Figure S4. Moreover, increased aberrations were seen when tankyrase inhibition and telomere damage induction were combined together, especially with regard to telomere association and mini-chromosome phenotypes (Figure 3E, Supplementary Figure S4). PARP1 inhibitor treated cells did not show the trend of increase in these telomere phenotypes compared to TNKS1 inhibition. In contrast, the PARP1 inhibitor

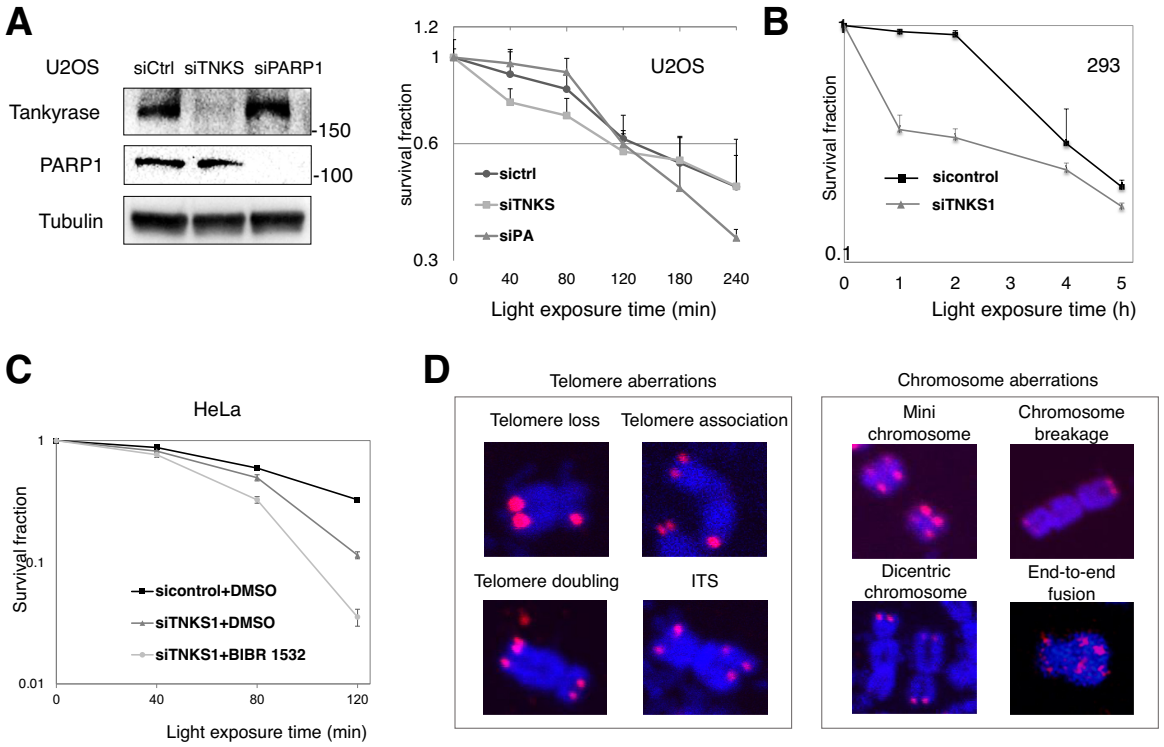

E

Treatment	Telomere aberrations				Chromosome aberrations			
	Telomere loss	Telomere association	Telomere doubling	ITS	Chromosome breakage	Mini chromosome	Dicentric chromosome	End-to-end fusion
HeLa1.3 DT1 DMSO (n = 1922)	4.9 %	1.9 %	1.1 %	3.4 %	2.0 %	4.2 %	3.4 %	0.02%
HeLa1.3 DT1 XAV939 (n = 1888)	9.3 %	2.2 %	1.6 %	3.8 %	1.4 %	7.3 %	2.1 %	0.00%
HeLa1.3 KT1 DMSO (n = 3790)	12.0 %	2.2 %	0.6 %	1.4 %	2.8 %	9.7 %	1.2 %	0.00%
HeLa1.3 KT1 XAV939 (n = 3176)	10.9 %	**2.6 %**	1.4 %	2.4 %	1.4 %	**11.4 %**	1.3 %	0.00%
HeLa1.3 DT1 Olaparib (n = 1590)	5.3%	0.21%	0.42%	0.03%	2.4%	2.9%	0.00%	0.00%
HeLa1.3 KT1 Olaparib (n = 2126)	4.5%	0.41%	0.40%	0.48%	2.4%	4.1%	0.04%	**0.14%**

Figure 3. TNKS1 is important for maintaining genome stability and cell survival after telomeric oxidative damage. (**A**) Colonigenic formation assay of U2OS cells that transiently expressed KT2, treated with sicontrol, siPARP1, or siTNKS1 and exposed to the indicated light exposure time. WB of PARP1 and TNKS1 expression is shown. (**B**) MTT assay of 293 cells that stably expressed KT1, treated with the indicated light exposure time. Mean values with a SE from three independent experiments are given. (**C**) Colonigenic formation assay of HeLa cells that transiently expressed KT2, exposed to the indicated light exposure time. The telomerase inhibitor BIBR 1532 was added to culture medium at a final concentration of 20 uM. (**D**) Representative images of metaphase spreads hybridized with Cy3 telomeric PNA probe. HeLa 1.3 cells stably expressing DT1 or KT1 were treated with DMSO, Olaparib or XAV939. Cells were then exposed to light for 1 h and recovered in the dark for 12 h before mitotic shake off and hybridization. Percentage of aberrations per chromosome is quantified in the right panel. Over 1921 chromosomes were scored. (**E**) Quantification of the frequency of telomere and chromosomal aberrations after treatment with Olaparib or XAV939.

leads to a small percentage of end-to-end chromosomal fusions that are not identified in the cells treated with the TNKS inhibitor (Supplementary Figure S4). This result indicated a higher level of telomere and genome instability in tankyrase-inhibited cells after telomeric damage, which may contribute to the increased cell death observed in Figure 3C.

TNKS1-mediated PARylation recruits the SSB repair machinery at damaged telomeres

Since TNKS1 is responsible for the telomeric damage-induced PAR (Figure 2), which is believed to be an early signal to recruit the SSB repair machinery (31), we tested the effect of TNKS1 on the downstream repair factors. First, we examined the recruitment of XRCC1 using different PARP inhibitors as described in Figure 2A. Telomeric damage induced by KT1 or non-telomeric damage induced by laser microirradiation, respectively, was carried out in the same cell to exclude cell heterogeneity. GFP-XRCC1 and Lig III were recruited efficiently to both KT1-induced telomere damage sites (Figure 4A, Supplementary Figure S5A) and 405 nm laser-induced genomic damage sites. Both responses were greatly blocked by PJ34, confirming the PAR-dependent recruitment of XRCC1 at both telomeric and genomic damage sites (Figure 4A and B). However, Olaparib did not have any effect on the DDR of XRCC1 at KT1 telomeric damage sites, despite the fact that the recruitment of XRCC1 to 405 nm laser-induced genomic damage sites was completely diminished in the same cell (Figure 4A, E). Consistently, knockout of PARP1 in MEF cells abolished the recruitment of XRCC1 to genomic damage sites but not to telomeric damage sites (Figure 4B). These data indicated that in contrast to the DDR at genomic damage sites, the recruitment of XRCC1 to telomeric damage sites does not rely on PARP1/2. On the other hand, when we treated cells with G007-LK or XAV939, the recruitment of XRCC1 to telomere damage sites was greatly impaired (Figure 4A, C and D). A similar result was observed for the recruitment of GFP-Polβ to KT1 sites (Figure 4C). The frequencies of XRCC1 and Polβ at telomere damage sites treated with XAV939 are quantified in Figure 4D. Furthermore, KD of TNKS1 reduced the recruitment of XRCC1 and Polβ to KT2 damage sites significantly (Figure 4E), reinforcing the importance of TNKS1 in recruiting downstream SSBR factors to damaged telomeres.

To further confirm that the loading of XRCC1 at telomeres depends on PAR, we analyzed the recruitment of the mutated XRCC1 LI360/361DD, which abolishes its binding with PAR polymer (4). We found that this mutant did not respond either to genomic damage induced by laser micro-irradiation or to telomeric damage induced by KT1 (Figure 4F). This data indicated that the recruitment of XRCC1 strongly depends on PAR at both telomeric and non-telomeric regions. These results indicate XRCC1 recruitment to telomeres depends on PAR activation but is independent of PARP1. The recruitment of various XRCC1 deletions at damaged telomeres is shown in Supplementary Figure S5B–D. As expected, the recruitment of XRCC1 to KT1 is dependent on its BRCTI domain, which has been reported to interact with ADP-ribose polymers, and this recruitment is suppressed by a tankyrase inhibitor but not a PARP1 inhibitor.

In addition, we tested the effect of SSBR deficiency on cell viability in U2OS cells. We found that knockdown of XRCC1 could sensitize cells to telomeric oxidative damage while knockdown of TNKS1 sensitized cells at a low damage dose, suggesting an initiation role of TNKS1 in telomere SSBR. Moreover, TNKS1 and XRCC1 double knockdown led to cell death in response to telomere oxidative damage (Figure 4G). In summary, unlike the genomic damage response, the recruitment of SSBR factors to telomere oxidative damage sites is initiated mainly by TNKS1-mediated PARylation rather than PARP1.

The ANK domain of TNKS1 is responsible for the TRF1 interaction and damage response at damaged telomeres

A question raised in our observations above is why cells choose different poly-ADP-polymerases for repair at different damage sites across chromatin. Since telomeres form unique T-loop structures and are coated with the shelterin complex, chromatin at telomeres is highly condensed, SSBs at damaged telomeres may be hard to expose and be detected by PARP1. The interaction between TNKS1 and TRF1 gave us a hint that TRF1 may play an important role in the recruitment of TNKS1 at telomere damage sites. TNKS1 comprises four distinct domains: an amino-terminal domain composed of homopolymeric runs of His, Pro, and Ser (the HPS domain); an ANK domain containing 24 ankyrin repeats which are important for its interaction with target proteins; a sterile alpha module (SAM) which may be involved in its homo-dimerization; and a C-terminal catalytic PARP domain (Figure 5A). Based on this structure, we constructed three truncations of TNKS1 and tagged them with GFP to test their damage response at telomere damage sites. We found that the ANK domain could interact with TRF1 extensively (Figure 5B) and respond to telomeric damage almost as efficiently as full length TNKS1 (Figure 5C). However, the SARP domain containing an SAM motif and the PARP domain, which could not interact with TRF1 efficiently (Figure 5B), also shows a damage response to telomeric damage (Figure 5C). Considering that endogenous TNKS1 may interfere with our observation by interacting with the SARP domain through its SAM motif, we further treated cells with siTNKS1 to exclude such an effect. Knockdown of TNKS1 decreased foci formation of SARP1 at KT2 damage sites significantly (Figure 5C). Consistent with this result, the PARP domain, which only contains the C-terminal catalytic domain, could not be recruited to telomere damage sites efficiently (Figure 5C). These results indicate that the ANK domain is responsible for both the interaction with TRF1 and the recruitment of TNKS1 to telomere damage sites.

TRF1 13-RGCADG-18 motif is essential for the interaction with, and recruitment of, TNKS1 to telomere damage sites and the subsequent telomere SSBR

Domain analysis of TNKS1 suggested a critical role of TNKS1-TRF1 interaction in the telomere damage response. To further confirm this, we explored the key residues

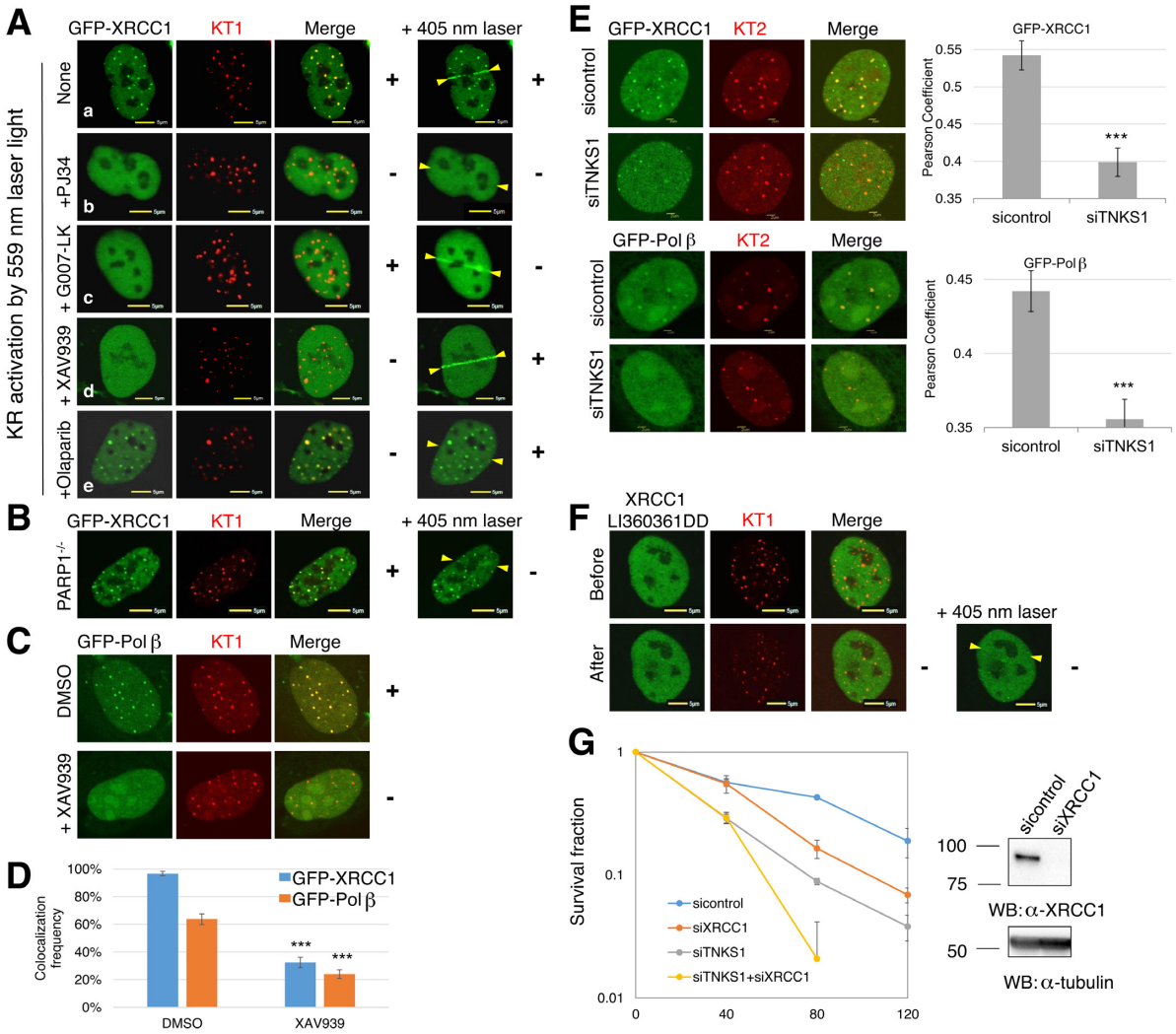

Figure 4. TNKS1-mediated PARylation is necessary for the recruitment of XRCC1 and Polβ at telomeric damage. (**A**) The recruitment of GFP-XRCC1 at telomeric damage is suppressed by the TNKS inhibitor G007-LK and XAV939 but not the PARP1 inhibitor Olaparib. U2OS cells were transfected with GFP-tagged XRCC1 and KT1. U2OS were pre-treated with 4 μM PJ34 for 30 min, 10 μM Olaparib for 2 h, 92 nM G007-LK for 24 h or 20 μM XAV939 for 24 h before 559 nm laser light was used to activate KT1 to induce telomeric damage. The same cell was then irradiated with 405 nm laser light exposure for 100 ms, indicated with yellow arrowheads. (**B**) MEF PARP1-/- cells were transfected with GFP-XRCC1 and KR-TRF1. Images at 3 min after laser irradiation are shown. (**C**) The recruitment of GFP-XRCC1 at telomeric damage is suppressed by the TNKS inhibitor XAV939. U2OS cells were transfected with GFP-tagged GFP-Polβ and KT1. Cells were exposed to light for 20 min and recovered in the dark for 30 min before fixation. (**D**) Quantification of colocation frequency of GFP-XRCC1 and GFP-Polβ at KT1 sites. Error bar represents over 50 cells. (**E**) Knockdown of TNKS1 reduces the recruitment of XRCC1 at telomere damage sites. U2OS cells were transfected with siTNKS1 or sicontrol and then transfected with GFP-XRCC1. Twenty-four hours post-transfection, cells were exposed to light for 20 min and recovered in the dark for 30 min. Pearson co-efficiency was quantified to analyze the recruitment of the protein. Mean values with an SE from over 100 telomeres are given. (**F**) Knockdown of TNKS1 reduces the recruitment of Polβ at telomere damage sites. Experiment procedure is similar to E. Mean values with an SE from over 129 telomeres are given. (F) Colonigenic formation assay of U2OS cells that transiently expressed KT2 exposed to the indicated light exposure time. Cells were treated with siXRCC1 or siTNKS1 or the double knockdown. Western blot of XRCC1 KD efficiency is shown on the right panel.

on TRF1 that are essential for its interaction with TNKS1. TNKS1 is widely expressed in cells and is implicated in a broad range of cellular processes such as Wnt signaling (41), telomere length regulation, lung fibrogenesis, and myelination (42). Among various substrates of TNKS1, a consensus motif containing an RGCADG hexapeptide has been found to be important for their binding to the peptide pocket of TNKS1 (43,44). In addition, a variant of this motif in the human TRF1 acidic domain has been identified to be critical for its interaction with TNKS1 in an *in vitro* GST-pull down assay (44). A Gly18Ala substitution at position 6 of its RGCADG motif disrupted the interaction between the TRF1 acidic domain and TNKS1 (44), and recently, this motif has been visualized in the interaction interface of the TNKS1-TRF1 complex crystal structure (45). Based on previous studies, we made a mutant TRF1 which contains the RG to AA mutation at the 13-**RG**CAD**G**-18 Tankyrase Binding Motif (TBM) (Figure 6A). A co-IP experiment indicated that the interaction between TRF1 and TNKS1 is greatly diminished by this TBM mutant. Also, this TBM

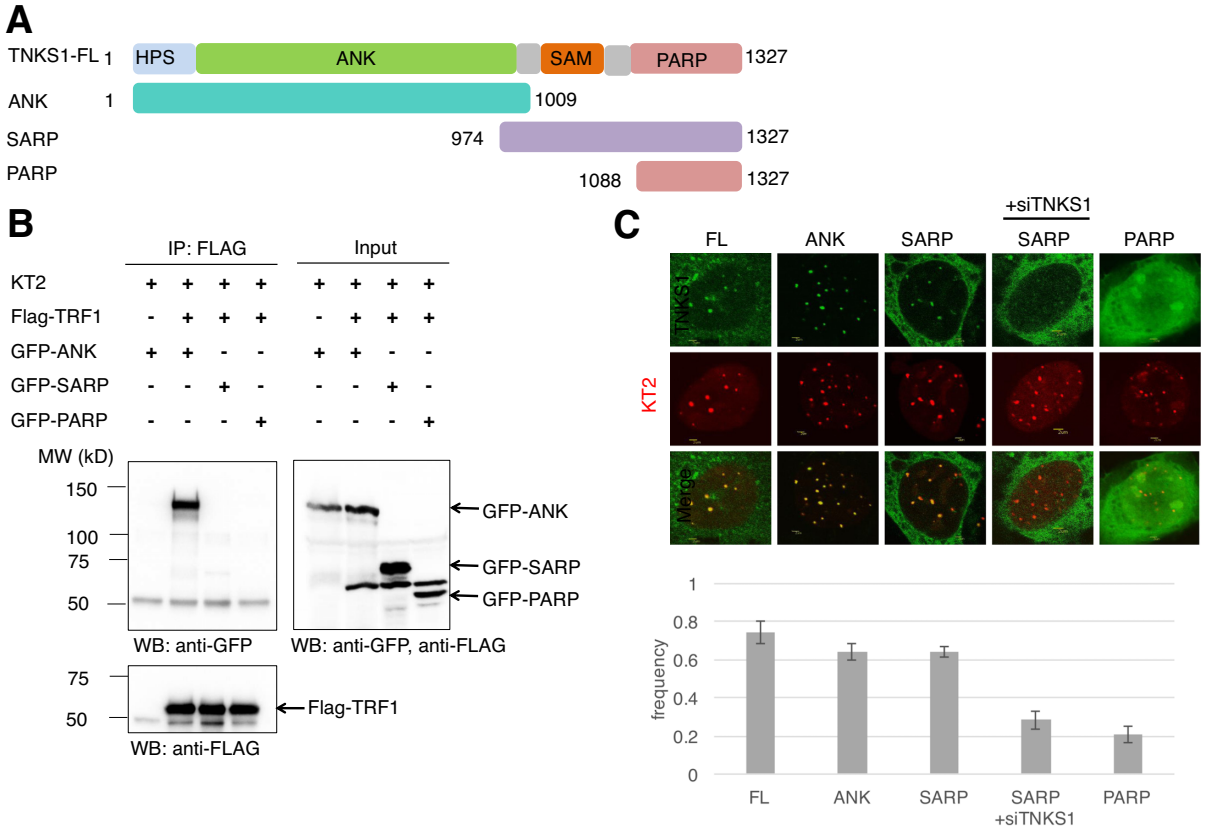

Figure 5. ANK domain is indispensable for the recruitment of TNKS1 at telomere damage sites. (**A**) Scheme of TNKS1 domains. Three truncations of TNKS1 were made and indicated in the scheme and tagged to a pEGFPC1 vector. (**B**) ANK of TNKS1 interacts with TRF1. KT2 expressing 293 cells were transfected with each indicated GFP-TNKS1 domain and FLAG-TRF1. Cell lysates were collected after light exposure for 10 min and immunoprecipitated with α-FLAG. The precipitates were immunoblotted with α-FLAG and α-GFP. (**C**) Recruitment of individual TNKS1 domains in KT2 expressing U2OS cells after light exposure for 10 min with or without siTNKS1 pretreatment. Quantification of the percentage of the co-localization of each TNKS1 domain with KT2-induced telomeric damage is shown. Error bar represents over 200 KT2 spots.

mutant was barely PARylated upon telomere damage compared to TRF1 wild type (WT) (Figure 6B). The telomeric expression pattern of this TBM mutant shows an undisturbed telomere repeat binding affinity (Figure 6C).

We then examined the effect of this mutant on telomere SSBR. To exclude the effect of endogenous TRF1, we treated cells with siTRF1 targeted at the 3′-UTR region. As shown in Figure 6C, knockdown of TRF1 reduced the recruitment of endogenous tankyrase at telomere damage sites significantly. TRF1 knockdown efficiency was confirmed by a western blot (Supplementary Figure S6A). When we overexpressed TRF1 WT in the siTRF1-pretreated cells, the loading tankyrase could be rescued almost to the extent of the siControl group (Figure 6C). However, overexpression of the TBM mutant in these cells exhibits impaired recruitment of both tankyrase (Figure 6C) and subsequent repair factors such as XRCC1 (Figure 6D) and Polβ (Supplementary Figure S6B) to telomere damage sites. The recruitment of tankyrase and XRCC1 to telomere damage sites was scored by their co-localization with KT2 (Figure 6E). Most importantly, TBM overexpression greatly sensitized U2OS cells treated with siTRF1 to telomere oxidative damage compared to TRF1 WT (Figure 6F). Together, these results indicated that the N-terminal TBM motif of TRF1 is indispensable for its interaction with TNKS1 and is important for subsequent SSBR at telomere oxidative damage sites.

Finally, previous studies have pointed out that TNKS1 can PARylate TRF1 *in vitro*. PARylated TRF1 is released from telomeres and subsequently targeted for the ubiquitin degradation pathway to allow the access of telomerase (36,46). In our study, we saw the recruitment of TNKS1 to telomeres as well as PARylation of TRF1 upon damage induction. We thus examined if damage-induced PARylation would affect TRF1 stability. We treated 293 cells with cycloheximide and compared the degradation rate of TRF1 with or without telomere damage. As shown in Supplementary Figure S7A, TRF1 indeed underwent degradation through the proteasome pathway since MG132 prevented its degradation. However, we did not observe any changes in the degradation rate in the damaged or undamaged group (Supplementary Figure S7B). We also overexpressed TNKS1 in cells to mimic the damage scenario and exaggerated the effect, while knocking down TNKS1 to see the opposite effect. We observed a trend of increased TRF1 degradation in TNKS1 overexpressing cells and a decreased degradation rate in TNKS1 KD cells (Supplementary Figure S7C-D), indicating the possibility of a dynamic change in shelterin

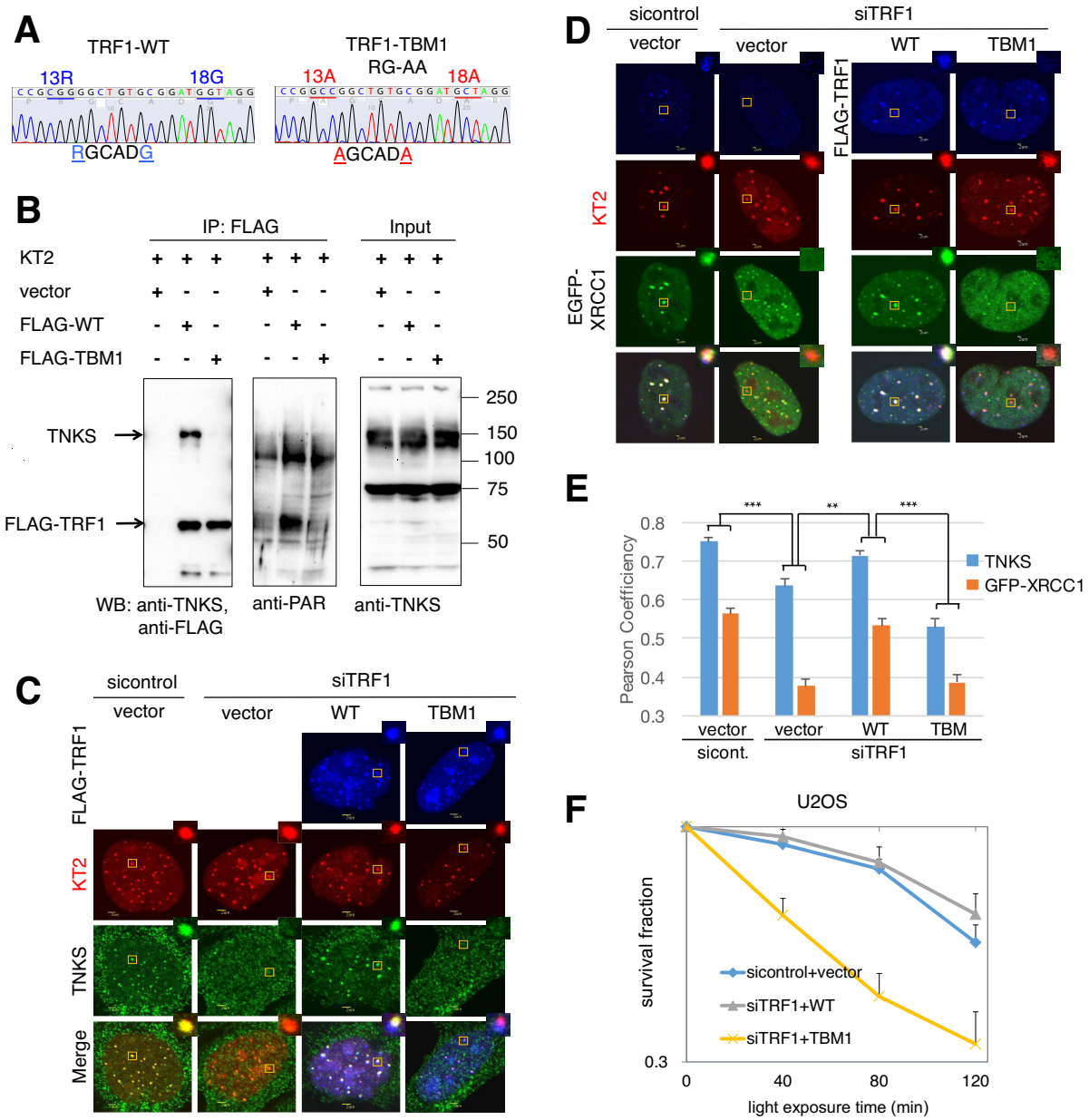

Figure 6. TBM mutant is necessary for PARylation-mediated repair initiation and cell survival upon telomeric damage. (**A**) Schematic illustration of TBM mutant. (**B**) TBM mutant does not interact with TNKS1 and affects PARylation after telomeric damage. 293 cells were co-transfected with KT2 and FLAG-TRF1 WT or TBM. Cell lysates were collected after light exposure for 10 min and immunoprecipitated with α-FLAG. The precipitates were immunoblotted with α-FLAG/tankyrase, PAR, and α-GFP. (C–E) Recruitment of TNKS1 (**C**) and GFP-XRCC1 (**D**) in siTRF1 pretreated KT2-expressing 293 cells with the expression of either FLAG-TRF1 WT or TBM. Pearson co-efficiency was quantified to analyze the recruitment of the protein. Mean values with an SE from over 300 telomeres are given (**E**). (**F**) Colonigenic formation assay of U2OS cells treated with sicontrol or siTRF1 and then transiently expressing KT2, exposed for the indicated time.

proteins when damage is induced at telomeres. Together, our data suggest that the recruitment of TNKS1 to telomere damage sites may be delicately regulated and fine-tuned, making it difficult to induce a dramatic change in TRF1 stability that can be observed through a macro-range method such as a western blot. However, more micro-ranged methods such as super-resolution microscopy might be helpful to capture more transient changes in a relatively short space and time window.

DISCUSSION

In this study, we demonstrated a novel mechanism for the initiation step of SSBR at telomere damage sites as opposed to genomic damage sites by utilizing the KR system to induce site-specific oxidative DNA damage. We found that TNKS1, a poly-ADP-polymerase, is recruited efficiently to telomere damage sites. Surprisingly, although PARP1 is responsible for the major activity of PAR in cells (31), treatment with the PARP1 inhibitor Olaparib did not have

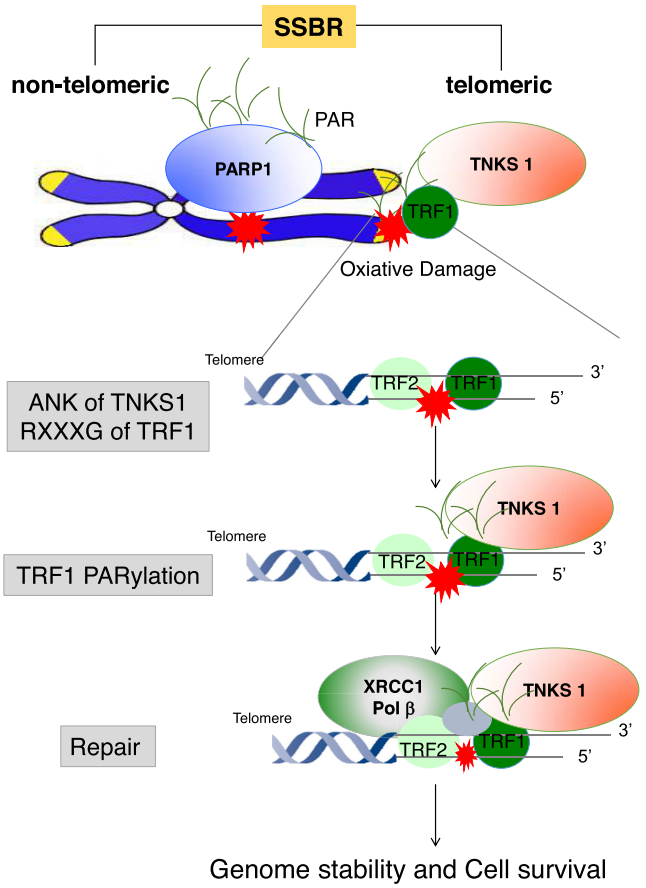

Figure 7. A model of poly ADP-ribosylation mediated by different proteins, at distinct genome loci, recruiting the oxidative damage repair machinery. Oxidative DNA damage at sites of the genome and telomeres facilitates the formation of PAR via PARP1 and TNKS1, respectively. TNKS1 is recruited to damaged telomeres through its interaction with TRF1. The interaction is dependent on the ANK domain of TNKS and the TBM motif of TRF1. Subsequent PARylation of TRF1 by TNKS1 recruits downstream repair proteins to sites of damage for repair, promoting genome stability and cell survival.

detectable effect on the recruitment of XRCC1 at telomere damage sites. On the contrary, treatment with TNKS-specific inhibitors or knockdown of TNKS1 greatly reduced the recruitment of XRCC1 and Polβ as well as PAR generation at telomere damage sites, indicating a role of TNKS1 in initiating SSBR at damaged telomeres. Furthermore, our results showed that the recruitment of TNKS1 to telomere damage sites is dependent on its interaction with the N-terminal TBM motif of TRF1. PARylation of TRF1 with the induction of telomere oxidative damage is mediated by TNKS1, and this poly-ADP polymer could serve as a signal to recruit downstream SSBR factors. Disrupting either step of this repair pathway could greatly sensitize cells to telomere oxidative damage.

Although it has been reported that there is a basal level of constitutive interaction between TRF1 and TNKS1, only a small fraction of TNKS1 is localized to telomeres in the absence of telomere DNA damage (37). The low abundance of tankyrase in the nucleus may be a barrier for the efficient interaction of tankyrase1 with TRF1. Indeed, we also observed punctuated localization of tankyrase in cells, especially in the cytoplasm and around the nucleus (Figure 1). The conformation of the TRF1 homodimer on telomeric DNA is relatively flexible (16), and the twisted horseshoe shape of the dimerization domain provides a large surface area for interactions with other factors (47). Previous studies have shown that tankyrase can form polymers and the dissociation of the polymer is regulated by their auto-PARylation activity (48–50). One possibility is that PARylation of TNKS1 and TRF1 could alter the structure of both proteins, which in turn would increase the interaction between them. Further studies to investigate the translocation, polymerization, and structure of the TNKS1-TRF1 complex after damage might provide us with a deeper understanding of the increased interaction between TNKS1 and TRF1 at telomeres after damage.

Although TNKS1 and PARP1 belong to the same protein family and have the same catalytic function, the way they act may not be the same. Here, we found a role for TNKS1 in facilitating telomere SSBR through its interaction with the TBM motif of TRF1. Inhibition of PARP1 pharmacologically or by knockout of PARP1 in MEF cells does not affect the recruitment of XRCC1 at telomeric oxidative damage sites (Figure 5). PARP1 has also been shown to be involved in telomere length regulation, telomere protection and maintenance of chromosome stability (51–53). An increase of chromosome end to end fusions was reported in PARP1 deficient primary murine cells (53). We also observed the end to end fusions in Olaparib treated but not TNKS inhibitor treated cells (Figure 3 and Supplementary Figure S4C). These results indicate that PARP1 might be involved in telomere protection after damage rather than TRF1 pARylation and regulation of SSBR. TRF2 localizes at telomeres and its telomere binding domain, Myb, is not recognized by PARP1 (53,54). Additionally, other shelterin proteins like Rap1 can also repress the recruitment of PARP1 to telomeres (55). However, PARP1 was found to co-localize with TRF2 when cells were exposed to DNA damaging reagents or at eroded telomeres (53). In fact, PARP1 was found to interact with the Myb domain of TRF2, which is also the DNA binding domain and might be exposed after damage. A recent report has shown that without the repression of RAP1 and TRF2^{B}, PARP1 can promote HDR resection at telomeres with other HR factors, resulting in massive telomere loss and telomere-free chromosome fusions (55). In addition, studies have shown a function of PARP1 in mediating A-NHEJ when C-NHEJ was repressed at DSBs (10,56). Our results indicate that PARP1 inhibition led to cell sensitivity especially after high dose damage in ALT cells (Figure 3A), supporting the idea that PARP1 plays a role in promoting repair for DSBs. On the other hand, a recent report showed that DNA LIG III but not PARP1 can act as a DNA strand break sensor associated with topoisomerase I inhibitor, supporting the existence of a second damage-sensing mechanism in SSBR involving the detection of nicks in the genome by LIG III (57). Our results suggest an unknown mechanism of SSBR initiation at telomeres mediated by TNKS1 rather than PARP1. This may be due to different damage types that these two PARPs prefer, different structures and chromosome backgrounds they encounter at distinct genomic sites, and/or

functional segregation of the two enzymes at telomeres. Together with TNKS1, PARP1 may participate in alt-NHEJ at telomeres, but this is not contradictory to our result. The function of PARP1 may need the involvement of other shelterin proteins or other factors, while the target for PARyaltion may not be TRF1 or may not be the same site of tankyrase-mediated PAR on TRF1. In this manuscript, we identified the role of TNKS1 in telomere SSBR through TRF1 and its contribution to cell survival, without excluding the role of PARP1 in protecting telomeres in other pathways.

The role of T-loop formation at telomeres is to protect chromosome ends from being detected as DSBs by the DNA repair machinery. However, a T-loop can also impede the progression of the replication fork, thus posing a replication stress at telomeres. Apart from this, the G-quadruplex formed by the G-rich telomeric sequence makes telomeres more vulnerable to replication stress (58,59). Based on the unique characteristics of the telomere, one possible explanation of increased cell death associated with telomere SSBR deficiency is that unrepaired SSBs at telomeres may be easier to transform to DSBs when encountered by the replication fork, making the SSB a more deleterious damage type at telomeres compared to non-telomeric regions (60). Another possible explanation would be the disruption of normal T-loop structure caused by damaged termini at SSBs, leading to the failure to protect the telomere. In either case, we should be able to see more DSB-related chromosome aberrations when inhibiting tankyrase during telomere oxidative damage. However, this is not likely to be the case since we did not detect any increase of the chromosome end-to-end fusion phenotype in HeLa 1.3 KT1 cells treated with a tankyrase inhibitor. Although an increase in overall chromosome aberrations, especially telomere associations and mini-chromosomes in cells containing telomeric damage with tankyrase inhibition, was observed (Figure 3E, Supplementary Figure S4), how these aberrations would affect cell viability and the detailed mechanism accounting for the increased cell death induced by tankyrase inhibition after telomere damage needs to be further explored.

While most human cancers express telomerase activity, approximately 10–15% maintain their telomeres through the ALT pathway. It is noteworthy that ALT cells seem to be more sensitive to telomere oxidative damage when treated with siTNKS1 compared to telomerase-positive cells (Figure 3A–C). Telomeres in ALT cells may not be as stable as in telomerase-positive cells. It is reported that in addition to the canonical TTAGGG repeat sequence in telomeres, variant repeat sequences including TCAGGG, TTCGGG, and GTAGGG are also found in ALT cells, owing to recombination events with upstream subtelomeric sequences (61). This may decrease the binding affinity of TRF1 and TRF2 to telomeres, since the Myb domains of TRF1 and TRF2 show very low tolerance for single-base changes (17). This would create a less condensed chromatin state at telomeres in ALT cells compared to telomerase-positive cells. Consistently, many chromatin remodelers that function in nucleosome deposition are reported to be frequently absent in ALT cells, including ATRX and ASF1 (61). It might be reasonable for ALT cells to loosen their telomeres as to increase telomere mobility, which would drive a homology search for recombination-dependent telomere elongation (62) and probably allow an assembly of the large protein complex that is required for such an event. However, the less compacted telomeres in ALT cells may also render them more vulnerable to DNA damage sources such as oxidative stress. Another possibility is that the greater sensitivity in ALT cells observed here (Figure 3A–C) may be due to lack of telomerase in ALT cells. In telomerase-positive cells, treatment with a telomerase inhibitor combined with siTNKS1 further increased cell sensitivity upon telomere damage (Figure 3C). Telomerase is important for maintaining telomere length and it accounts for the unlimited cell growth of 85–90% of tumor cells (63,64). Studies have shown that inhibition of telomerase in cancer cells would lead to progressive telomere shortening and limited proliferation, as well as increased cell senescence (65). In addition, knockout of telomerase in mice would lead to increased mortality after a few generations (66). Interestingly, double knockout of Ku86 or DNA-PKCs with telomerase magnified the mortality of the mice compared to single depletion of telomerase, supporting the notion that absence of telomerase and short telomeres in combination with DNA repair deficiencies accelerates the aging process without impacting tumorigenesis (66). Consistently, our data has shown a synergistic effect of TNKS and telomerase inhibition on the survival of HeLa cells when cells are challenged by telomeric oxidative damage (Figure 3C). These data suggest that telomerase may be needed for processing the eroded telomeres caused by oxidative damage, especially in cells lacking efficient repair machineries due to TNKS KD. The role of telomerase in mitigating telomere shortening might rescue cell death since telomerase could heal the telomeres that have become truncated due to oxidative damage. Future studies are needed to elucidate the mechanisms by which telomerase contributes to cell survival after oxidative DNA damage.

In summary, our results revealed a novel function of TNKS1 in the DNA damage response at telomeres, preserving telomere integrity. Based on the above observations, we propose the model in Figure 7. When oxidative DNA damage is induced at telomeres, TNKS1 is recruited to the damage sites through its interaction with TRF1, subsequently PARylating TRF1 and recruiting SSBR machinery at telomeres, which is important for genome stability and cell survival. We have also defined the critical amino acids in TRF1 which are responsible for its interaction with TNKS1. The damage signaling pathway and DSB repair machinery have been thought to be repressed at functional telomeres. Moreover, recent studies have shown that some proteins involved in the repair pathway are also associated with the shelterin complex and may be involved in end processing and T-loop formation after replication, suggesting that functional telomeres can be recognized as DNA breaks during a temporally limited window (13,20,67). The repair machinery for the DNA breaks at telomeres may not be simply repressed but must be well-regulated in order to maintain a functional telomere at different cell stages and damage states. Here, we have demonstrated the mechanism of SSBR at telomeric oxidative damage sites. The low dose sensitization shown in cancer cells (Figure 3B) indicates that TNKS1 could be a potential target for effective cancer ther-

apy with less toxicity. Moreover, inhibition of telomerase is not as effective as expected in cancer treatment due to a lag phase for critically short telomeres to ultimately induce cell growth arrest or cell death (68). Thus, combination of TNKS and telomerase inhibitors might be a promising strategy to increase cell killing efficacy. It would also be interesting to how DSBs are repaired at telomeres and how the balance between damage repair and end protection is achieved and regulated. Our findings provided the initial mechanistic distinction between DSB repair at damaged telomere and chromosomal sites and suggest that telomeres might be a promising target for cancer therapy.

SUPPLEMENTARY DATA

Supplementary Data are available at NAR Online.

ACKNOWLEDGEMENTS

We thank Dr Susan Smith for providing FLAG-tankyrase1 and Rong Tan for her discussion of results in the project.
Contributions: L.Y. and L.S. performed the major experiments, Y.T., H.C. and Y.G. provided help with the experiments. A.S.L. discussed the interpretation of results and aided in the entire work. S.N. and L.L. designed the experiments. L.Y., L.S. and L.L. wrote the manuscript. All authors helped in editing the manuscript.

FUNDING

National Institutes of Health (NIH) [AG045545 and GM118833 to L.L.]; China Scholarship Council (to L.S., L.Y.); UPCI Imaging Facility and UPCI Cytometry Facility were provided by the Cancer Center Support Grant from the National Institutes of Health [P30 CA047904]. Funding for open access charge: NIH [GM118833].
Conflict of interest statement. None declared.

REFERENCES

1. Caldecott,K.W. (2008) Single-strand break repair and genetic disease. *Nature reviews. Genetics*, **9**, 619–631.
2. Okano,S., Lan,L., Caldecott,K.W., Mori,T. and Yasui,A. (2003) Spatial and temporal cellular responses to single-strand breaks in human cells. *Molecular and cellular biology*, **23**, 3974–3981.
3. Lan,L., Nakajima,S., Oohata,Y., Takao,M., Okano,S., Masutani,M., Wilson,S.H. and Yasui,A. (2004) In situ analysis of repair processes for oxidative DNA damage in mammalian cells. *Proceedings of the National Academy of Sciences of the United States of America*, **101**, 13738–13743.
4. El-Khamisy,S.F., Masutani,M., Suzuki,H. and Caldecott,K.W. (2003) A requirement for PARP-1 for the assembly or stability of XRCC1 nuclear foci at sites of oxidative DNA damage. *Nucleic acids research*, **31**, 5526–5533.
5. Wei,L., Nakajima,S., Hsieh,C.L., Kanno,S., Masutani,M., Levine,A.S., Yasui,A. and Lan,L. (2013) Damage response of XRCC1 at sites of DNA single strand breaks is regulated by phosphorylation and ubiquitylation after degradation of poly(ADP-ribose). *J Cell Sci*, **126**, 4414–4423.
6. Marintchev,A., Robertson,A., Dimitriadis,E.K., Prasad,R., Wilson,S.H. and Mullen,G.P. (2000) Domain specific interaction in the XRCC1-DNA polymerase beta complex. *Nucleic acids research*, **28**, 2049–2059.
7. Caldecott,K.W., McKeown,C.K., Tucker,J.D., Ljungquist,S. and Thompson,L.H. (1994) An interaction between the mammalian DNA repair protein XRCC1 and DNA ligase III. *Molecular and cellular biology*, **14**, 68–76.
8. Caldecott,K.W. (2003) XRCC1 and DNA strand break repair. *DNA repair*, **2**, 955–969.
9. Oei,S.L., Keil,C. and Ziegler,M. (2005) Poly(ADP-ribosylation) and genomic stability. *Biochem Cell Biol*, **83**, 263–269.
10. Sfeir,A. and de Lange,T. (2012) Removal of shelterin reveals the telomere end-protection problem. *Science*, **336**, 593–597.
11. O'Sullivan,R.J. and Karlseder,J. (2010) Telomeres: protecting chromosomes against genome instability. *Nat Rev Mol Cell Biol*, **11**, 171–181.
12. Cesare,A.J. and Reddel,R.R. (2010) Alternative lengthening of telomeres: models, mechanisms and implications. *Nature reviews. Genetics*, **11**, 319–330.
13. de Lange,T. (2004) T-loops and the origin of telomeres. *Nature reviews. Molecular cell biology*, **5**, 323–329.
14. de Lange,T. (2005) shelterin: the protein complex that shpes and safeguards human telomeres. *Genes and Development*, **12**, 47–56.
15. Palm,W. and de Lange,T. (2008) How shelterin protects mammalian telomeres. *Annu Rev Genet*, **42**, 301–334.
16. Bianchi,A., Stansel,R.M., Fairall,L., Griffith,J.D., Rhodes,D. and de Lange,T. (1999) TRF1 binds a bipartite telomeric site with extreme spatial flexibility. *The EMBO journal*, **18**, 5735–5744.
17. Hanish,J.P., Yanowitz,J.L. and de Lange,T. (1994) Stringent sequence requirements for the formation of human telomeres. *Proceedings of the National Academy of Sciences of the United States of America*, **91**, 8861–8865.
18. Opresko,P.L., Fan,J., Danzy,S., Wilson,D.M. 3rd and Bohr,V.A. (2005) Oxidative damage in telomeric DNA disrupts recognition by TRF1 and TRF2. *Nucleic acids research*, **33**, 1230–1239.
19. Deng,Y., Chan,S.S. and Chang,S. (2008) Telomere dysfunction and tumour suppression: the senescence connection. *Nat Rev Cancer*, **8**, 450–458.
20. Longhese,M.P. (2008) DNA damage response at functional and dysfunctional telomeres. *Genes and Development*, **22**, 125–140.
21. Sfeir,A., Kabir,S., van Overbeek,M., Celli,G.B. and de Lange,T. (2010) Loss of Rap1 induces telomere recombination in the absence of NHEJ or a DNA damage signal. *Science*, **327**, 1657–1661.
22. Blasco,M.A. (2005) Telomeres and human disease: ageing, cancer and beyond. *Nature reviews. Genetics*, **6**, 611–622.
23. Levy,M.Z. (1992) Telomere end-replication problem and cell aging. *J Mol Biol*, **225**, 951–960.
24. Sun,L., Tan,R., Xu,J., LaFace,J., Gao,Y., Xiao,Y., Attar,M., Neumann,C., Li,G.M., Su,B. *et al.* (2015) Targeted DNA damage at individual telomeres disrupts their integrity and triggers cell death. *Nucleic acids research*, **43**, 6334–6347.
25. Simone Petersen,T.V.Z. (1998) Preferential Accumulation of single-stranded regions in telomeres of human fibroblasts. *Experimental cell research*, **239**, 152–160.
26. Coluzzi,E., Colamartino,M., Cozzi,R., Leone,S., Meneghini,C., O'Callaghan,N. and Sgura,A. (2014) Oxidative stress induces persistent telomeric DNA damage responsible for nuclear morphology change in mammalian cells. *PLoS One*, **9**, e110963.
27. Lan,L., Nakajima,S., Wei,L., Sun,L., Hsieh,C.L., Sobol,R.W., Bruchez,M., Van Houten,B., Yasui,A. and Levine,A.S. (2014) Novel method for site-specific induction of oxidative DNA damage reveals differences in recruitment of repair proteins to heterochromatin and euchromatin. *Nucleic acids research*, **42**, 2330–2345.
28. Remington,S.J. (2006) Fluorescent proteins: maturation, photochemistry and photophysics. *Curr Opin Struct Biol*, **16**, 714–721.
29. Bulina,M.E., Chudakov,D.M., Britanova,O.V., Yanushevich,Y.G., Staroverov,D.B., Chepurnykh,T.V., Merzlyak,E.M., Shkrob,M.A., Lukyanov,S. and Lukyanov,K.A. (2006) A genetically encoded photosensitizer. *Nat Biotechnol*, **24**, 95–99.
30. Bulina,M.E., Lukyanov,K.A., Britanova,O.V., Onichtchouk,D., Lukyanov,S. and Chudakov,D.M. (2006) Chromophore-assisted light inactivation (CALI) using the phototoxic fluorescent protein KillerRed. *Nature protocols*, **1**, 947–953.
31. Ame,J.C., Spenlehauer,C. and de Murcia,G. (2004) The PARP superfamily. *BioEssays : news and reviews in molecular, cellular and developmental biology*, **26**, 882–893.
32. Smith,S., Giriat,I., Schmitt,A. and de Lange,T. (1998) Tankyrase, a poly(ADP-ribose) polymerase at human telomeres. *Science*, **282**, 1484–1487.

33. Cook,B.D., Dynek,J.N., Chang,W., Shostak,G. and Smith,S. (2002) Role for the Related Poly(ADP-Ribose) Polymerases Tankyrase 1 and 2 at Human Telomeres. *Molecular and cellular biology*, **22**, 332–342.
34. Carpentier,P., Violot,S., Blanchoin,L. and Bourgeois,D. (2009) Structural basis for the phototoxicity of the fluorescent protein KillerRed. *FEBS Lett*, **583**, 2839–2842.
35. Buettner,G.R. (1993) The spin trapping of superoxide and hydroxyl free radicals with DMPO (5,5-dimethylpyrroline-N-oxide): more about iron. *Free Radic Res Commun*, **19**(Suppl. 1), S79–S87.
36. Smith,S. and de Lange,T. (2000) Tankyrase promotes telomere elongation in human cells. *Curr Biol*, **10**, 1299–1302.
37. Smith,S. and de Lange,T. (1999) Cell cycle dependent localization of the telomeric PARP, tankyrase, to nuclear pore complexes and centrosomes. *J Cell Sci*, **112**, 3649–3656.
38. Nagy,Z., Kalousi,A., Furst,A., Koch,M., Fischer,B. and Soutoglou,E. (2016) Tankyrases Promote Homologous Recombination and Check Point Activation in Response to DSBs. *PLoS genetics*, **12**, e1005791.
39. Narwal,M., Venkannagari,H. and Lehtio,L. (2012) Structural basis of selective inhibition of human tankyrases. *Journal of medicinal chemistry*, **55**, 1360–1367.
40. Li,N., Zhang,Y., Han,X., Liang,K., Wang,J., Feng,L., Wang,W., Songyang,Z., Lin,C., Yang,L. *et al.* (2015) Poly-ADP ribosylation of PTEN by tankyrases promotes PTEN degradation and tumor growth. *Genes & development*, **29**, 157–170.
41. Zhang,Y., Liu,S., Mickanin,C., Feng,Y., Charlat,O., Michaud,G.a., Schirle,M., Shi,X., Hild,M., Bauer,A. *et al.* (2011) RNF146 is a poly(ADP-ribose)-directed E3 ligase that regulates axin degradation and Wnt signalling. *Nature cell biology*, **13**, 623–629.
42. Riffell,J.L., Lord,C.J. and Ashworth,A. (2012) Tankyrase-targeted therapeutics: expanding opportunities in the PARP family. *Nat Rev Drug Discov*, **11**, 923–936.
43. Guettler,S., LaRose,J., Petsalaki,E., Gish,G., Scotter,A., Pawson,T., Rottapel,R. and Sicheri,F. (2011) Structural basis and sequence rules for substrate recognition by Tankyrase explain the basis for cherubism disease. *Cell*, **147**, 1340–1354.
44. Sbodio,J.I. and Chi,N.W. (2002) Identification of a tankyrase-binding motif shared by IRAP, TAB182, and human TRF1 but not mouse TRF1. NuMA contains this RXXPDG motif and is a novel tankyrase partner. *The Journal of biological chemistry*, **277**, 31887–31892.
45. Li,B., Qiao,R., Wang,Z., Zhou,W., Li,X., Xu,W. and Rao,Z. (2016) Crystal structure of a tankyrase 1-telomere repeat factor 1 complex. *Acta Crystallogr F Struct Biol Commun*, **72**, 320–327.
46. Chang,W., Dynek,J.N. and Smith,S. (2003) TRF1 is degraded by ubiquitin-mediated proteolysis after release from telomeres. *Genes and Development*, **17**, 1328–1333.
47. Fairall,L., Chapman,L., Moss,H., de Lange,T. and Rhodes,D. (2001) Structure of the TRFH dimerization domain of the human telomeric proteins TRF1 and TRF2. *Mol Cell*, **8**, 351–361.
48. Sbodio,J.I., Lodish,H.F. and Chi,N.W. (2002) Tankyrase-2 oligomerizes with tankyrase-1 and binds to both TRF1 (telomere-repeat-binding factor 1) and IRAP (insulin-responsive aminopeptidase). *Biochem J*, **361**, 451–459.
49. De Rycker,M. and Price,C.M. (2004) Tankyrase polymerization is controlled by its sterile alpha motif and poly(ADP-ribose) polymerase domains. *Mol Cell Biol*, **24**, 9802–9812.
50. DaRosa,P.A., Ovchinnikov,S., Xu,W. and Klevit,R.E. (2016) Structural insights into SAM domain-mediated tankyrase oligomerization. *Protein Sci*, **25**, 1744–1752.
51. d'Adda di Fagagna,F., Hande,M.P., Tong,W.M., Lansdorp,P.M., Wang,Z.Q. and Jackson,S.P. (1999) Functions of poly(ADP-ribose) polymerase in controlling telomere length and chromosomal stability. *Nat Genet*, **23**, 76–80.
52. Beneke,S., Cohausz,O., Malanga,M., Boukamp,P., Althaus,F. and Burkle,A. (2008) Rapid regulation of telomere length is mediated by poly(ADP-ribose) polymerase-1. *Nucleic acids research*, **36**, 6309–6317.
53. Gomez,M., Wu,J., Schreiber,V., Dunlap,J., Dantzer,F., Wang,Y. and Liu,Y. (2006) PARP1 Is a TRF2-associated Poly(ADP-Ribose)Polymerase and Protects Eroded Telomeres. *Molecular Biology of the Cell*, **17**, 1686–1696.
54. Court,R., Chapman,L., Fairall,L. and Rhodes,D. (2005) How the human telomeric proteins TRF1 and TRF2 recognize telomeric DNA: a view from high-resolution crystal structures. *EMBO Rep*, **6**, 39–45.
55. Rai,R., Chen,Y., Lei,M. and Chang,S. (2016) TRF2-RAP1 is required to protect telomeres from engaging in homologous recombination-mediated deletions and fusions. *Nat Commun*, **7**, 10881.
56. Badie,S., Carlos,A.R., Folio,C., Okamoto,K., Bouwman,P., Jonkers,J. and Tarsounas,M. (2015) BRCA1 and CtIP promote alternative non-homologous end-joining at uncapped telomeres. *EMBO J*, **34**, 410–424.
57. Abdou,I., Poirier,G.G., Hendzel,M.J. and Weinfeld,M. (2015) DNA ligase III acts as a DNA strand break sensor in the cellular orchestration of DNA strand break repair. *Nucleic Acids Res*, **43**, 875–892.
58. Bochman,M.L., Paeschke,K. and Zakian,V.A. (2012) DNA secondary structures: stability and function of G-quadruplex structures. *Nature reviews. Genetics*, **13**, 770–780.
59. Zimmermann,M., Kibe,T., Kabir,S. and de Lange,T. (2014) TRF1 negotiates TTAGGG repeat-associated replication problems by recruiting the BLM helicase and the TPP1/POT1 repressor of ATR signaling. *Genes & development*, **28**, 2477–2491.
60. Kuzminov,A. (2001) Single-strand interruptions in replicating chromosomes cause double-strand breaks. *Proceedings of the National Academy of Sciences of the United States of America*, **98**, 8241–8246.
61. Episkopou,H., Draskovic,I., Van Beneden,A., Tilman,G., Mattiussi,M., Gobin,M., Arnoult,N., Londono-Vallejo,A. and Decottignies,A. (2014) Alternative Lengthening of Telomeres is characterized by reduced compaction of telomeric chromatin. *Nucleic acids research*, **42**, 4391–4405.
62. Cho,N.W., Dilley,R.L., Lampson,M.A. and Greenberg,R.A. (2014) Interchromosomal homology searches drive directional ALT telomere movement and synapsis. *Cell*, **159**, 108–121.
63. Kim,N.W., Piatyszek,M.A., Prowse,K.R., Harley,C.B., West,M.D., Ho,P.L., Coviello,G.M., Wright,W.E., Weinrich,S.L. and Shay,J.W. (1994) Specific association of human telomerase activity with immortal cells and cancer. *Science*, **266**, 2011–2015.
64. Smogorzewska,A. and de Lange,T. (2004) Regulation of telomerase by telomeric proteins. *Annu Rev Biochem*, **73**, 177–208.
65. Damm,K., Hemmann,U., Garin-Chesa,P., Hauel,N., Kauffmann,I., Priepke,H., Niestroj,C., Daiber,C., Enenkel,B., Guilliard,B. *et al.* (2001) A highly selective telomerase inhibitor limiting human cancer cell proliferation. *EMBO J*, **20**, 6958–6968.
66. Espejel,S., Klatt,P., Menissier-de Murcia,J., Martin-Caballero,J., Flores,J.M., Taccioli,G., de Murcia,G. and Blasco,M.A. (2004) Impact of telomerase ablation on organismal viability, aging, and tumorigenesis in mice lacking the DNA repair proteins PARP-1, Ku86, or DNA-PKcs. *J Cell Biol*, **167**, 627–638.
67. Zhu,X.D., Kuster,B., Mann,M., Petrini,J.H. and de Lange,T. (2000) Cell-cycle-regulated association of RAD50/MRE11/NBS1 with TRF2 and human telomeres. *Nat Genet*, **25**, 347–352.
68. Cerone,M.A., Londono-Vallejo,J.A. and Autexier,C. (2006) Telomerase inhibition enhances the response to anticancer drug treatment in human breast cancer cells. *Mol Cancer Ther*, **5**, 1669–1675.